Journal of Digital Imaging

3D Bicipital Groove Shape Analysis and Relationship to Tendopathy

Aaron D. Ward,[1] Ghassan Hamarneh,[1] and Mark E. Schweitzer[2]

The bicipital groove of the proximal humerus is formed by the medial and lateral tuberosities and serves to retain the long biceps tendon in its proper place as the arm moves. Bicipital root and proximal tendon disorders are an important symptom generator in the shoulder. The accuracy of the diagnosis of many shoulder disorders visually without quantitative shape analysis is limited, motivating a clinical need for some ancillary method to assess the proximal biceps. In previous studies, measurements of bicipital groove shape were 2-dimensional (2D), taken from a single axial slice. Because of significant variations in groove shape from one axial slice to another in a single patient, such approaches risk overlooking shape features important to long biceps tendon pathology. In this paper, we present a study of the relationship between bicipital groove shape and long biceps tendon pathology using a novel 3-dimensional (3D) shape descriptor for the bicipital groove. In addition to providing quantitative measures of the shape of the groove and its relation to tendopathy, the new descriptor allows for intuitive, descriptive visualization of the shape of the groove.

KEY WORDS: Bicipital groove, intertubercular sulcus, long biceps tendon, musculoskeletal disorder, 3D shape analysis

INTRODUCTION

The bicipital groove (BG) of the proximal humerus is a groove in the humeral head formed by the medial and lateral tuberosities (Fig. 1). The long biceps tendon (LBT) sits within the BG; the BG prevents the LBT from dislocating during movement of the arm. Bicipital root and proximal tendon disorders are becoming increasingly recognized as an important symptom generator in the shoulder. The spectrum of abnormalities includes tenosynovitis, pulley lesions, SLAP tears, biceps dislocations, and proximal tears. The BG and the LBT are intimately related; the shape of the BG can have a great impact on the tendency for the LBT to be dislocated, subluxated, frayed, or torn. It is understood that a shallow, wide BG can promote subluxation and/or dislocation of the LBT, a deep, narrow BG can cause LBT irritation and tenosynovitis, osseous spurs in the BG can cause LBT fraying, and the presence of the supratubercular ridge of Meyer is suspected to promote dislocation.[1–4]

Historically, the accuracy for the diagnosis of many of these disorders by imaging has been limited. Therefore, there is a clinical need for some ancillary method to assess the proximal biceps. Because of the long known interrelationship of the BG with several types of shoulder disorders, this is an obvious source of secondary data. Previous studies of BG shape variation primarily involved taking 2-dimensional (2D) measurements from a single axial cross section of the humerus[3–6] (Fig. 2). Because of the large variation in BG shape from one axial slice to the next within a single patient (Fig. 1c, d), such measurements risk overlooking shape features important to LBT pathology. This motivates the development of an approach to the 3-dimensional (3D) shape description of the BG; such a description is one of the main contributions of

[1]*From the Medical Image Analysis Lab, Simon Fraser University, Burnaby, BC, V5A 1S6, Canada.*

[2]*From the Department of Radiology and Orthopedic Surgery, NYU School of Medicine, Hospital for Joint Diseases, New York, NY, 10016, USA.*

Correspondence to: Aaron D. Ward, Medical Image Analysis Lab, Simon Fraser University, Burnaby, BC, V5A 1S6, Canada; e-mail: award@cs.sfu.ca

Online publication 7 March 2007
doi: 10.1007/s10278-007-9027-6

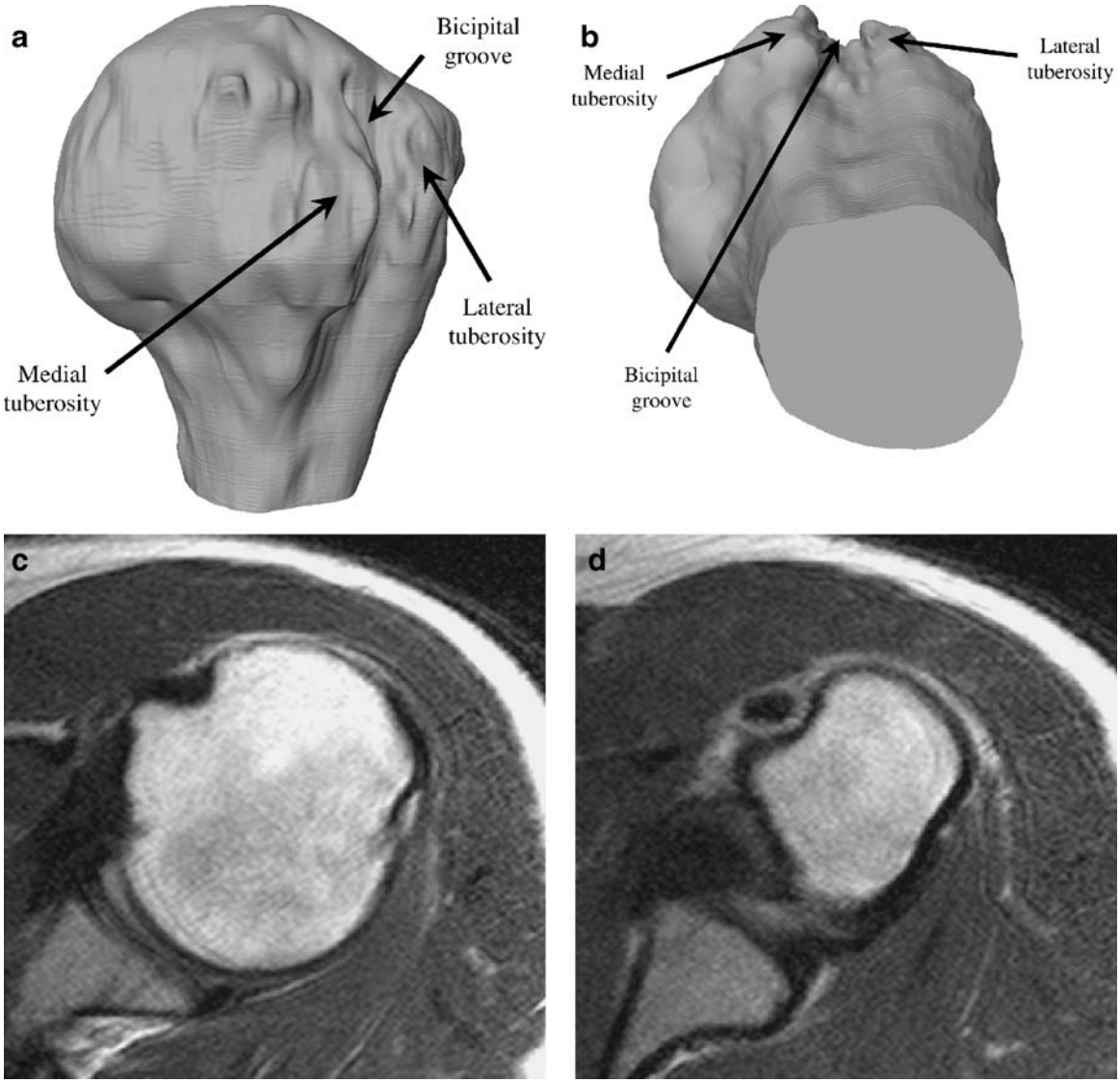

Fig 1. (a) Profile view of a humeral head (segmented from a MRI of the shoulder) with tuberosities and BG indicated. (b) View similar to Ahovuo's "groove view,"[6] showing the profile of the BG. (c) An axial slice from a 1.5-T MRI showing the BG. (d) A distal slice from the same patient, illustrating the large intrapatient variability in BG shape (the dark oval is the LBT).

this paper. Although the shape of the proximal humerus has been studied in 3D previously,[7,8] these studies are primarily concerned with capturing the shape of the humeral head for arthroplasty. Our target application differs from that of these previous works, and motivates a shape descriptor capturing different aspects of BG shape. Our work also differs in that our study is based on in vivo MR images, whereas the previous studies are based on excised humeri. Our shape description is inspired by medial axis-based shape representations, which are useful in anatomical applications because they intuitively capture bending, elongation, and thickening of shapes.[9,10] We validate the discriminatory power of our shape descriptor by testing the performance of different classifiers attempting to classify normal versus pathological BG shapes (defined according to established 2D measurements taken in previous literature).[3,4,6,11]

The other main contribution of this paper is a study of 32 images of patients presenting with various diagnoses of LBT pathology. In this study, we group the data sets according to expert diagnosis of LBT condition for each data set, and

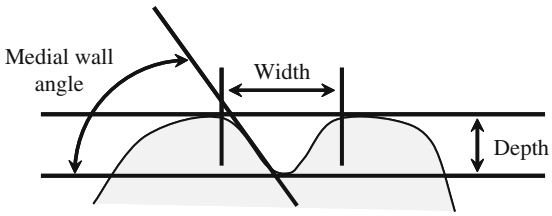

Fig 2. BG measurements taken from a single cross section in previous literature: medial wall angle, width, and depth.

use the 3D shape of their BGs to determine shape differences between the groups. We test the null hypothesis that the means of the groups are the same, rejecting it in favor of the alternative hypothesis that there are statistically meaningful differences in the 3D shapes in the normal group (ie, in subjects not having LBT pathology) compared to the pathological groups (ie, in subjects having a torn, subluxated, or dislocated LBT).

The remainder of this paper is organized as follows. In "Materials and Methods" we discuss the data sets we used, the computation of the proposed 3D shape descriptor and its validation, and the approach to computing shape differences between normal and pathological groups. In the "Results" section we give our experimental results, and discuss them in the "Discussion" section. Also in the Discussion section, we discuss the qualitative and quantitative visualization capabilities afforded by this shape representation. In the "Conclusion" section, we give some concluding remarks and future directions.

MATERIALS AND METHODS

In this section, we give an overview of the data sets involved in this study ("Materials"), the computation of the 3D shape representation for the BG ("3D Shape Representation") and its validation ("Validation of 3D Shape Representation), and the computation of shape attributes leading to calculation of the differences between the groups ("Computing Differences Between Groups").

Materials

We took 32 T2-weighted MR images of patients' shoulders at 1.5 T, with imaging parameters as follows: TR 4000–5500, TE 40–50, field of view (FOV) 14, matrix 256, slice thickness 4 mm. The mean age of the patients was 50 years (standard deviation 18.4 years), with the youngest patient being 24 and the oldest being 87 years of age. Of the 32 images, 19 were of male patients and 13 were of females. From these images, the bicipital groove surface was segmented manually by a graduate student under the direction of a board-certified radiologist. It was critical to distinguish between the cortical and endosteal surfaces during segmentation, to ensure that the surface that comes in contact with the LBT was the one extracted (Fig. 3). Based on the appearance of the LBT on MR, each patient was diagnosed by a board-certified radiologist to belong to one of the following six groups: normal, tear, subluxation, dislocation, tear and subluxation, and tear and dislocation. The criteria for the diagnoses are described in previous work.[12,13] This study was conducted under a waiver from the Institutional Review Board.

3D Shape Representation

Our goal is to develop a shape representation of the BG that captures its overall shape (not limited to a single slice), allows for quantitative 3D shape

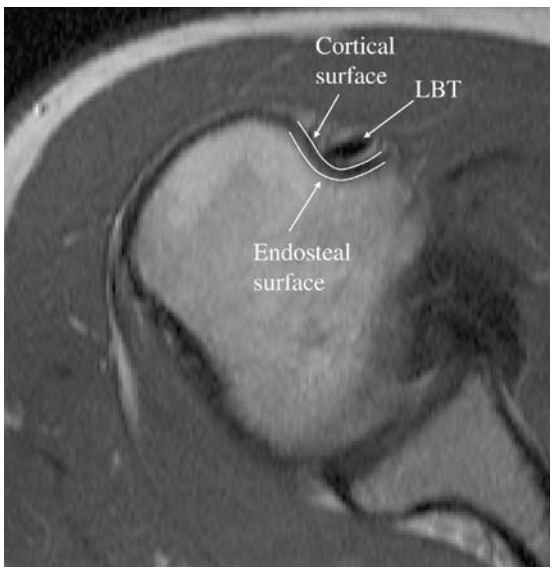

Fig 3. Appearance of bone on T2-weighted MRI. The inner surface where bone meets bone marrow is the endosteal surface. The outer surface where bone meets surrounding tissue is the cortical surface. We must distinguish between these during surface extraction, because the LBT contacts the cortical surface.

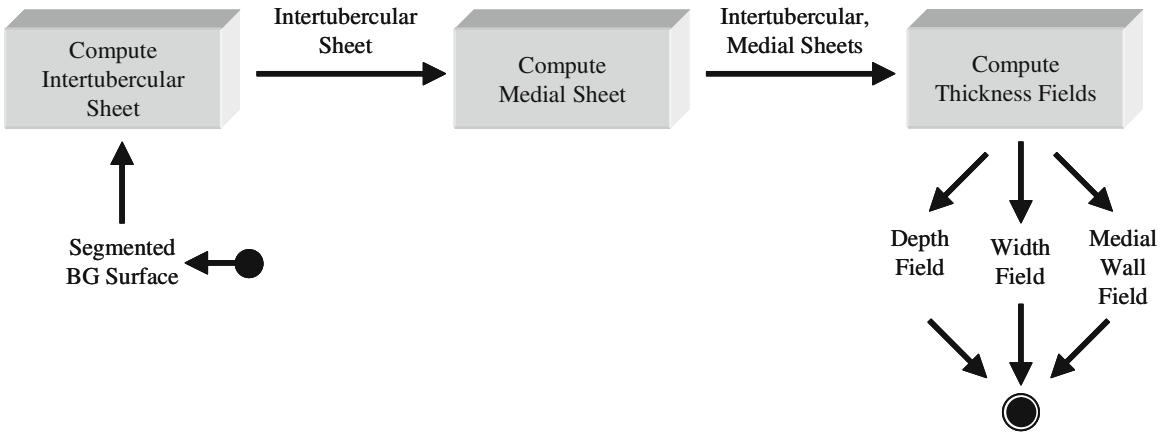

Fig 4. The pipeline used to compute the 3D shape representation proposed in this paper, a schematic of which is shown in Figure 6. Beginning with a segmented BG surface (Fig. 5a), we first compute the intertubercular sheet, which intersects both tuberosities and closes the BG (Fig. 5b). Next, we compute the medial sheet to lie perpendicular to the intertubercular sheet on each slice, and lie near the deepest region of the BG while remaining smooth (Fig. 5d). Lastly, we compute thickness fields (distance maps) from the medial sheet to form width and medial wall fields (an example of which is given in Fig. 11a), and from the intertubercular sheet to form a depth field.

measurements extending the 2D classical measurements, and allows for intuitive visualization and exploration of the BG. The process used to compute the 3D shape representation presented in this paper is given in Figure 4, and is as follows:

1. Compute intertubercular sheet. Starting with a BG surface (Fig. 5a), we automatically locate all of the points at the apexes of the tuberosities and define an *intertubercular sheet* to close the BG and intersect with these apexes (Fig. 5b). The purpose of the intertubercular sheet is to allow for the computation of the depth of the BG at any point. The depth of the BG at any point P on its surface is defined to be the length of the ray emanating from and perpendicular to the intertubercular sheet, ending at P (Fig. 6).
2. Compute medial sheet. Next, we compute the depth at every point on the BG based on the intertubercular sheet. We wish to use this depth information to position a *medial sheet*, perpendicular to the intertubercular sheet, along the deepest region of the BG. To clarify, this medial sheet is medial with respect to the BG; that is, it approximately bisects the groove extending distally from near the humeral head. However, this approach produces a discontinuous medial sheet (Fig. 5c). We define as the optimal path that which is as smooth as possible and at the same time as close to the deepest point (trough) of the groove as possible. We quantify these criteria using the following objective function:

$$C = \alpha D + \beta S,$$

where D is the BG depth, S is the smoothness of the curve defined by the path, and α and β are tuning parameters. The process of finding the optimal path minimizing this objective function can be divided into multiple stages, where each stage involves finding one point along the path in a single axial slice (ie, we proceed through the BG one axial slice at a time, choosing the optimal path on that slice; see Fig. 7). Having reformulated this problem as a multistage decision process, we can use a well-known algorithm in computing/optimization called *dynamic programming* to find the optimal path.[14] We obtained good results for all data sets by setting α=β=0.5. The dynamic programming method calculates the optimal path while reducing the number of computations required (as compared with a brute-force search for the optimal path). The medial sheet is computed to follow this optimal path and be perpendicular to the intertubercular sheet at each point where the medial sheet intersects the intertubercular sheet.
3. Compute thickness fields. Finally, the medial wall, width, and depth fields are computed (Fig. 6). Rays are cast from the medial wall and perpendicular to it, to the BG surface. For each point on the medial wall, its corresponding

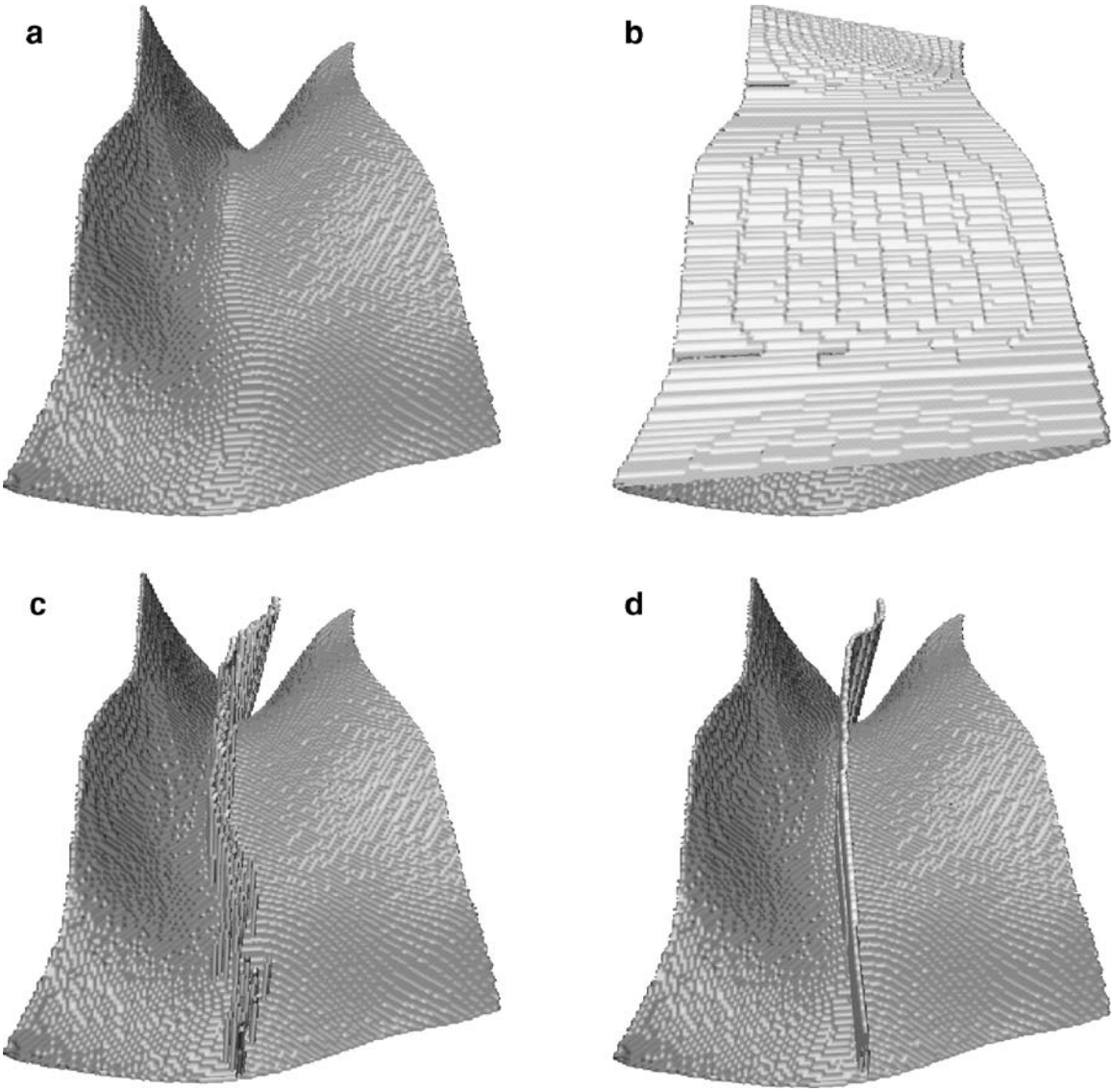

Fig 5. (a) The segmented surface of a BG. (b) Intertubercular sheet fitted to BG surface. (c) Medial sheet fitted using BG depth as the only criterion. Note discontinuities in the medial sheet. (d) Medial sheet fitted using BG depth and medial sheet smoothness as criteria, each with 50% weight. The medial sheet now lies generally in the deepest part of the BG while remaining smooth.

ray length is recorded. This forms a medial wall thickness field, an example of which is shown in Figure 11. This process is repeated, except that rays are cast toward both the medial and lateral BG walls, and the sum of their lengths in taken, forming a width field. The depth values computed previously for use in positioning the medial wall field can be reused to form a depth field. In all of the thickness fields, the distance between any two neighboring points is 0.1 mm. This resolution was chosen to be higher than that of the original 3D images, guaranteeing that the thickness fields capture the smallest features perceptible in the original images.

To summarize, we begin with a segmented BG surface consisting of a set of 3D points lying on the surface. From this, we compute a set of three thickness fields capturing information about the depth, width, and medial wall of the BG. These

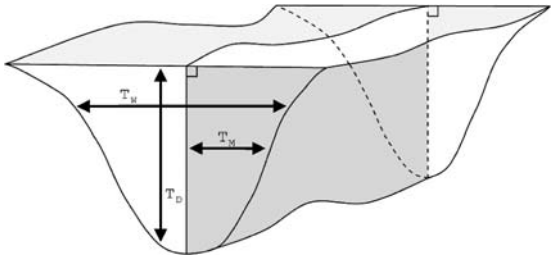

Fig 6. Schematic of a BG in 3D, to illustrate the computation of the thickness fields based on the intertubercular and medial sheets. T_D represents a single thickness value computed for the depth field. Note that depth is measured normal to the intertubercular sheet. T_W and T_M represent thickness values computed for the width and medial wall fields, respectively. Note that these thicknesses are measured normal to the medial sheet.

fields are computed to be the 3D analogues of the 2D depth, width, and medial wall angle BG measurements taken in previous studies (Fig. 2).

Validation of 3D Shape Representation

In this section, we seek to address the question of whether the proposed 3D shape representation can be used to diagnose the normality/pathology of the BG, as defined by distributions of 2D measurements taken of large numbers of bones in previous studies.[3,4,6] Previous studies typically take a single set of 2D measurements of width, depth, and medial wall angle for each BG, either from a dry bone or a radiograph. Additionally, previous researchers note the presence/absence of the supratubercular ridge of Meyer (henceforth referred to as "the ridge") on each BG, which is a ridge of bone projecting immediately proximal to the medial wall of the bicipital groove and continuous with it,[2] and is considered to have an impact on the tendency for dislocation of the LBT. These measurements of width, depth, medial wall angle, and presence/absence of the ridge shall henceforth be referred to as the "classical measurements" for brevity. Here, we test whether our shape representation captures, at minimum, the classical measurements. We are particularly interested in the ridge as its identification poses difficulty even for the expert observer.

The hypothesis is that indeed the proposed 3D shape descriptor captures the classical measurements. To test the hypothesis, we follow the process given in Figure 8:

1. Compute classical measurements. Given a set of points sampled from a segmented BG surface, we automatically compute the width, depth, and medial wall angle (Fig. 2) of each data set. To take the measurements, the BG surfaces are first rotated so that slicing along the axial direction yields cross sections orthogonal to the humerus. An intertubercular sheet is fitted to the tuberosities (Fig. 6). At each axial slice S, the intertubercular sheet appears as a line segment PQ with endpoints P and Q touching the tuberosities. The depth of the BG on S is determined as shown in Figure 9. The width of the BG at S is the length of PQ. Starting from the deepest point on the BG surface on S, points sampled along the medial wall define endpoints of line segments approximating the wall. Angles of these line segments with respect to the segment PQ are recorded for S. So, for each BG, we have a set of depth and width values and a set of medial wall angles. Since measurements taken in previous work are of a single slice, and previous authors are not specific in describing how the slice is chosen,[3,4,6] we aggregate all of our measurements by taking the mean for a single data set to yield a single depth, width, and medial wall angle for each data set. The choice of how to aggregate the data to best reflect the choices

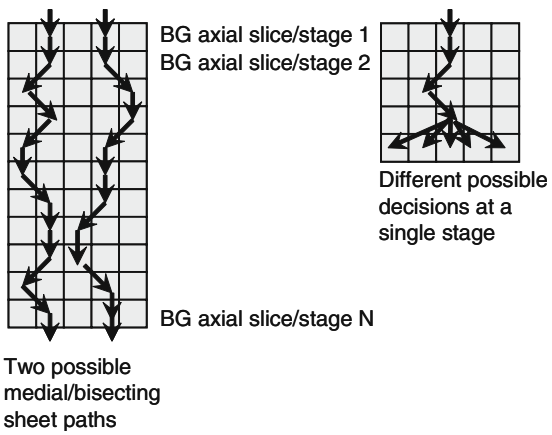

Fig 7. Figure depicting the stages of the dynamic programming process used to find the optimal path through the BG that maximizes criteria of depth and smoothness. Each axial slice of the BG is considered a single stage in the process wherein the best choice is made for the position of the medial sheet based on choices made in previous stages. The formulation of this problem as a multistage decision process enables the use of dynamic programming, which is computationally efficient.

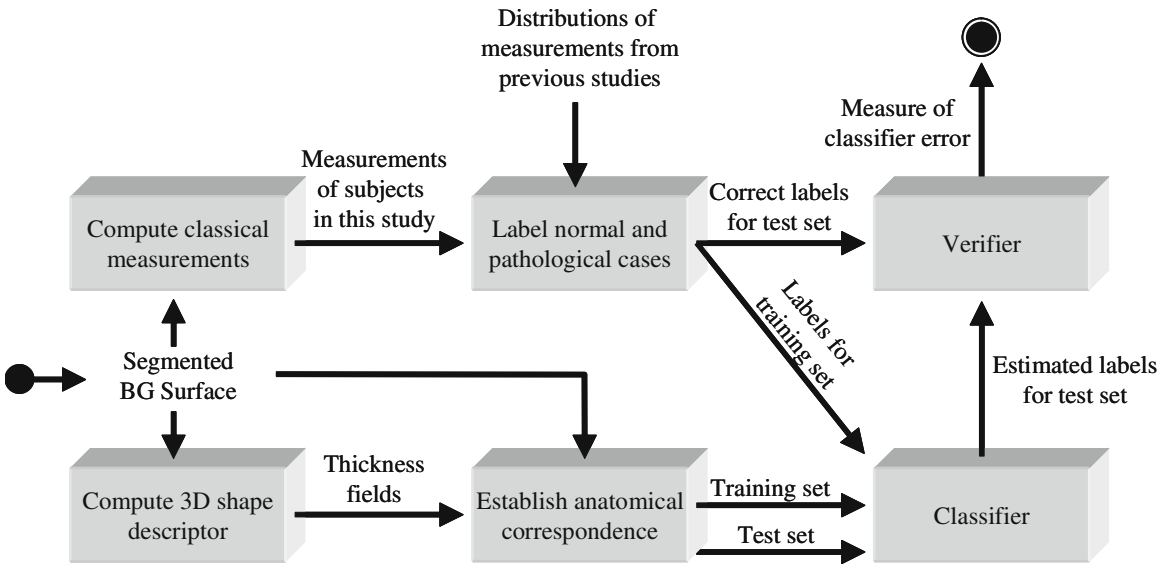

Fig 8. Process used to validate the proposed 3D shape descriptor. Points sampled from the surface of the BG are used to compute the descriptor (Fig. 6), and also used to compute "classical" measurements of BG shape used in previous work (Fig. 2). Based on distributions of classical measurements determined in previous studies, a diagnosis of normal versus pathological shape is made for each data set based on its classical measurements. These diagnoses form labels for a set of training shapes given to a classifier, which attempts to correctly label BG shapes in the test set. We evaluate the accuracy of the classifier based on a comparison of these labels to known labels for the test set.

made by previous researchers in measuring BGs is a difficult one because of the fact that it is not clear from where in the humerus the measurements were taken. This single-slice limitation further reinforces the need for a 3D shape descriptor, as different ways of aggregating the data yield different results.

2. Label normal and pathological cases. Three previous studies have performed measurements of depth, width, and medial wall angle on dry bones and radiographs.[3,4,6] Counting all of these studies, each measurement was taken on 130 bones. The results are as follows. Medial wall angle mean: 60.02°; standard deviation (SD): 15.32°; depth mean: 4.19 mm; SD: 0.96 mm; width mean: 7.9 mm; SD: 1.42 mm. Although it is understood that there is a relationship between BG shape and LBT pathology, the exact nature of this relationship is unknown. It is therefore not possible for an expert to label each training set as normal or pathological according to the shape of its BG; the exact nature of a pathological BG shape is currently unknown. For example, although it is known that a shallow, wide BG can promote LBT dislocation, it is not known precisely *how* shallow and *how* wide a BG has to be to guarantee LBT dislocation with high confidence. Consequently, we turn to previous studies taking measurements of the BG on dry bones and radiographs to obtain a mean and standard deviation (SD) of these measurements for a sample of the population, and specify a SD cutoff to distinguish normal from pathological cases for each measurement type. Although this classification seems arbitrary, as our objective here is to test the performance of a set of classifiers in distinguishing cases that are closer to normal (closer to the mean obtained from previous studies) from those which are closer to pathological (further from the mean obtained from previous studies), the choice of SD cutoff is more important in the relative sense of its effect on the training set than in an absolute sense of the exact value chosen. We choose a standard deviation threshold of 1.5 SD for our data, for all measurement types (ie, depth, width, medial wall angle). Thus, for example, if a data set's classical depth measurement is 1.5 SD further from the mean of the distribution of depth values reported in previous studies, it is deemed to be abnormal; otherwise

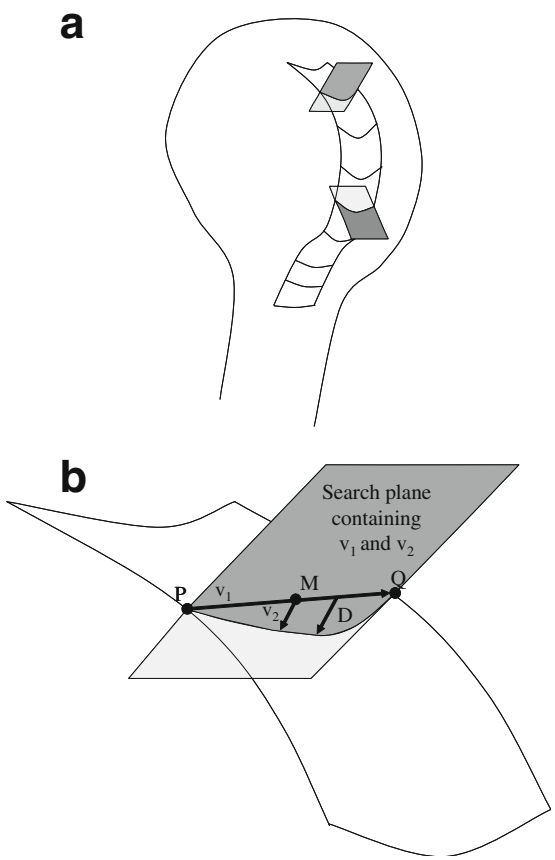

Fig 9. Because the BG curves with the contour of the humeral head, it is important in measuring depth to ensure that depth is measured along vectors orthogonal to the intertubercular sheet, lying in search planes exemplified in (a). (b) is an enlarged view of a single search plane from (a) showing the details of the definition of the search plane at a given slice of the BG. Segment *PQ* is defined to join the endpoints of the intertubercular sheet, and vector v_1 is defined from *P* to *Q*. Vector v_2 is defined to originate from the midpoint *M* of *PQ* and be normal to the intertubercular sheet at *M*. The search plane is defined to contain v_1 and v_2. Rays are cast from points sampled uniformly along and orthogonal to *PQ*, constrained to lie in the search plane, and terminating at the BG surface. The length of the longest such ray (indicated by *D*) is determined to be the depth of the BG on this slice.

it is normal. This threshold, applied to all measurement types, results in the following labeling: medial wall angle—15 normal data sets, 17 abnormal data sets; width—14 normal, 18 abnormal; depth—18 normal, 14 abnormal. The significance of this choice of threshold is the challenge that it presents to the classifier, as there are roughly as many normals as abnormals (47%, 44%, and 56% of the sets are normals for medial wall angle, width, and depth, respectively). For instance, a different choice of threshold could yield 30 normals and two abnormals. A classifier, which blindly classifies all test sets as normal, would achieve 30/32=93.8% accuracy. By choosing a suitable threshold we ensure that a classifier cannot achieve high accuracy by consistently outputting a single response. Each data set was also labeled according to observation, by a board-certified radiologist, of the supratubercular ridge of Meyer.[2]

3. Computation of 3D shape descriptor. This is computed as described in "3D Shape Representation," according to the process given in Figure 4.
4. Anatomical correspondence. To prepare the field data for classifiers, we establish anatomically meaningful correspondence between elements. Point (*i, j*) in any thickness field of a given type should correspond anatomically with points (*i, j*) in the thickness fields of the same type in all other data sets. Establishing

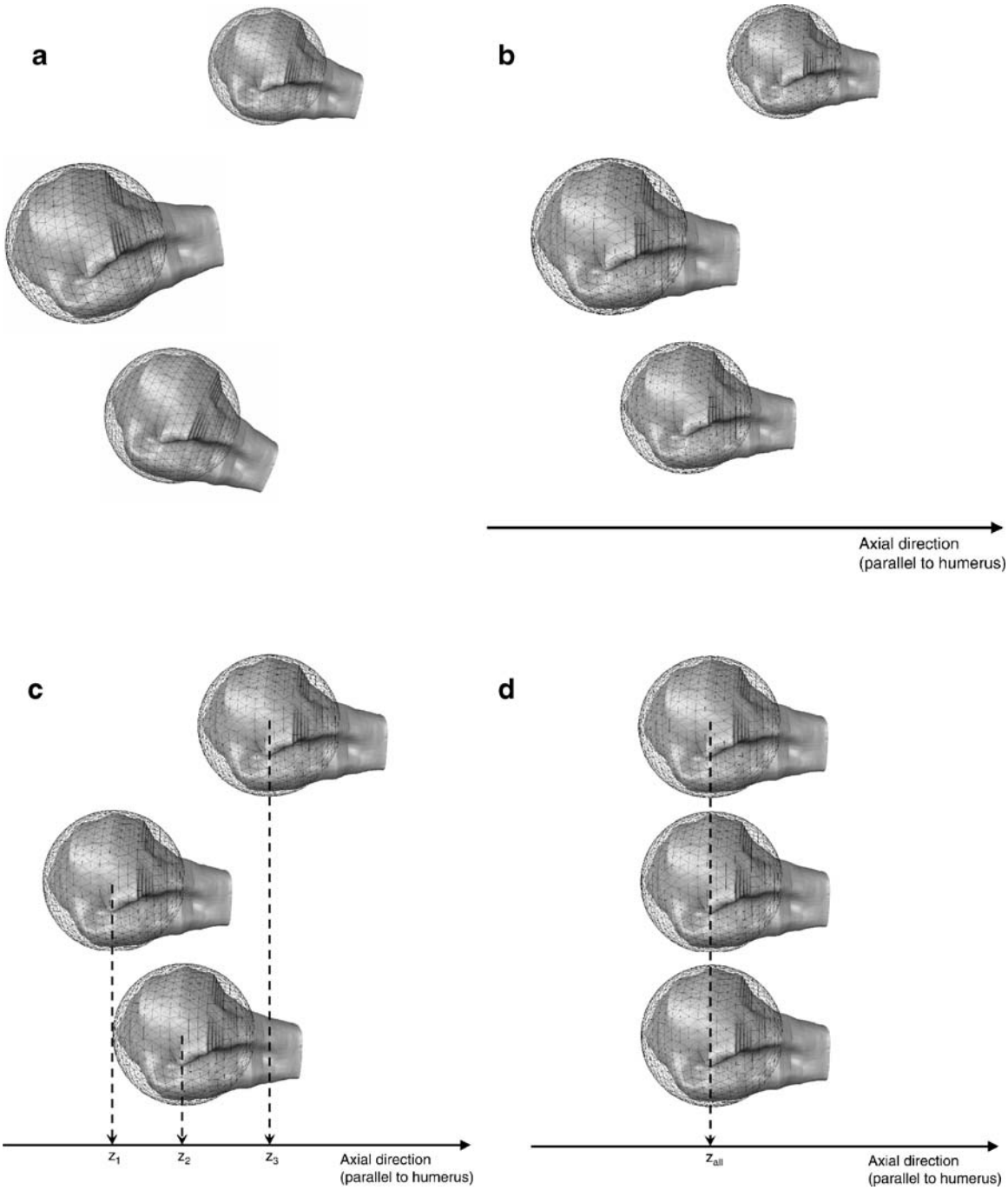

Fig 10. An illustration of the anatomical alignment process. (a) Unaligned humeri. (b) Three humeri of different sizes and at different positions along the axial dimension (to which the humerus is aligned). Wire mesh spheres fit to the humeral heads illustrate the size differences between the heads. (c) The same humeri after normalization of humeral head size. Note that the axial coordinates z_1, z_2, z_3 of the sphere centers are different. (d) The same humeri after alignment along the axial dimension. The axial coordinate of the sphere center is now the same for each humerus.

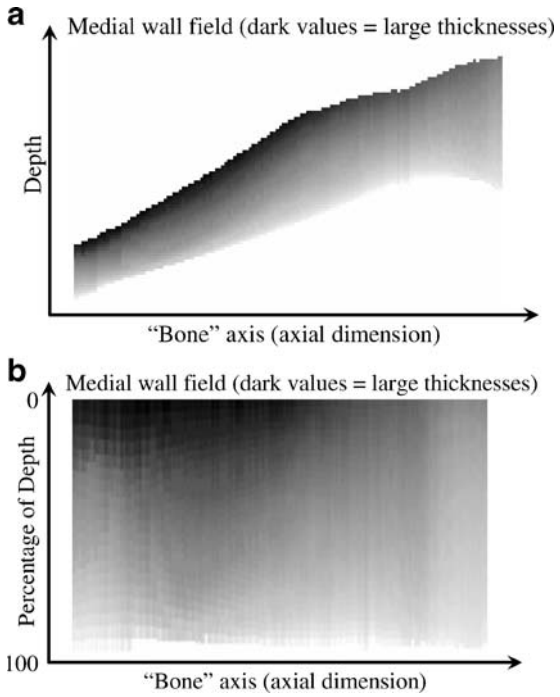

Fig 11. (a) A medial wall field rendered as a 2D image, with one axis along the bone (axial) dimension, and the other along the depth of the BG. (b) The same field after rescaling along the depth dimension to transform it into a "percentage of depth" dimension for alignment.

correspondence is challenging for the BG as it does not have well-defined anatomical landmarks. Because of large slice thickness, the proximal end of the BG is not reliably determined, and a method for reliably determining the distal end is debated.[4] Our approach avoids having to define the beginning and the end of the BG: since the BG is formed by parts of the humerus (tuberosities), we align the *humeri*, carrying alignment of the BGs along consequently. Our shape descriptor is invariant to rigid transformations except translation along the axial dimension (recall that all BG surfaces are rotated so that the humerus is axially aligned), and it is not invariant to changes in scale. To establish correspondence, we compute the center and radius of the best-fit sphere to points sampled on the humeral head using the Hough transform.[15] The Hough Transform yields a score for each of a large number of candidate spheres, centered at different locations and with different radii. The score for a given sphere is proportional to the number of humeral head points through which its surface passes. We choose the sphere with the largest such score. The alignment process that follows is given in Figure 10. We uniformly scale thickness fields to normalize for humeral head size (Fig. 10c), using the best-fit sphere radii as the indicator. We align all thickness fields such that the axial coordinate of these spheres is the same, thus aligning the bones (Fig. 10d). Our rationale is that we need an approach to alignment that is based on

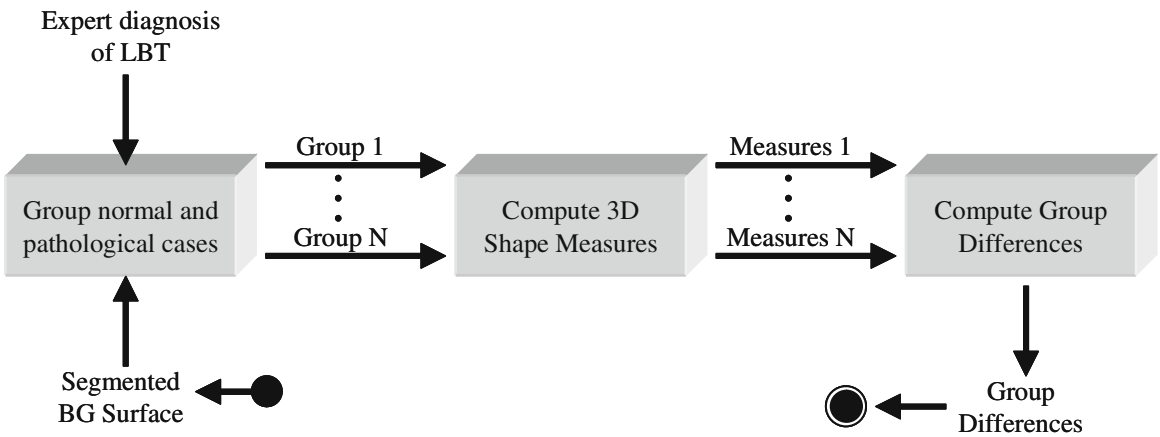

Fig 12. Process used to compute differences between groups having normal versus pathological LBTs. First, we compute the 3D shape descriptor from the segmented BG surface. Next, each data set is assigned a group label by an expert who has diagnosed the LBT based on the reading of the original MRI, resulting in *N* different groups (eg, normal, tear, subluxation, dislocation, etc.). 3D shape measures are then computed for each group, and they are compared to determine their differences.

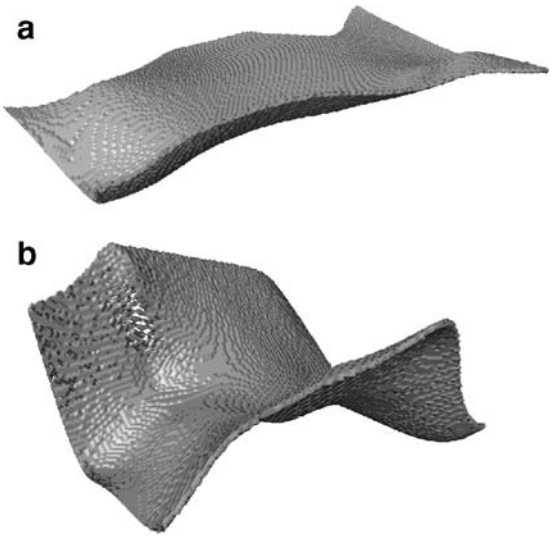

Fig 13. (a) An example of a BG with a large elongation (λ_1/λ_2) score of 16.1. (b) A BG with a much smaller elongation score of 3.1.

humeral anatomical landmarks, accounts for different-sized bones, and aligns the grooves axially without relying on poorly defined groove boundaries along the axial dimension. To the best of our knowledge, an approach to alignment meeting these criteria does not exist in the literature. For example, Procrustes Alignment,[16] a widely used approach, aligns the shapes such that the sum of the distances of each shape to the mean shape is minimized. For our application, this approach to alignment would result in a scaling of the thickness fields so that they are normalized to each other without respect to the size of the humeral head. It would similarly adversely affect the translation of each thickness field along the axial dimension. The essential need for an application-specific approach to alignment for this anatomy is that accurate alignment must take into account information about anatomy (humeral head) other than that directly under study (bicipital groove). After alignment, we have a set of thickness fields (eg, Fig. 11a), normalized for scale and aligned along the bone (axial) dimension. The final step is a rescaling of the field along the depth dimension to make the fields rectangular by resampling thickness values at locations from 0% to 100% along the depth of the BG (Fig. 11b).

5. Classification. Because each thickness field includes 1,000 thickness values, it can be regarded as a multivariate observation with 1,000 variables. We perform principal components analysis[17] on the thickness fields to avoid performing supervised classification against such large observations. We then trained several classifiers against the principal components of the depth, width, and medial wall field data capturing 95% of the variation. We also trained classifiers to recognize the presence/absence of the supratubercular ridge of Meyer[2] based on the depth fields. Because of our small sample size, testing of the classifiers was performed in a leave-one-out fashion, with classification errors averaged over all rounds.

Computing Differences Between Groups

In this section, we describe our method for computing 3D BG shape differences between groups of patients with normal LBTs, compared with groups having various LBT abnormalities (eg, tear, subluxation, dislocation, etc.). The process is given in Figure 12 and is as follows:

Table 1. Results of Validation of the Proposed 3D Shape Descriptor

	Classifier	Error	No. Principal Components
Width	Quadratic Bayes	0.1875	6
Depth	Min. LS Linear	0.1875	6
Medial wall angle	Quadratic Bayes	0.3750	15
Supratubercular ridge	Min. LS Linear	0.1250	6

The methods shown gave the best performance against our data. Each row corresponds to a single type of measurement (width, depth, medial wall angle) or observation (presence or absence of supratubercular ridge). The second column shows the classifier yielding the best performance in performing a correct diagnosis of the normality/pathology of the given measurement. The third column shows the classification error rate, and the fourth column shows the number of principal components used (after principal components analysis is performed on the BG surfaces) to train the classifiers.

Table 2. Results of 3D Shape Measures Taken Against the Bicipital Groove Surfaces

	Elongation	Surface Roughness	3D Moment
Normal	6.4	4.4	3.0×10^7
Tear	6.3	3.1	7.7×10^6
Subluxation	11.3	2.9	9.0×10^6
Dislocation	7.3	3.5	1.1×10^7
Tear and Subluxation	13.2	3.6	1.6×10^7
Tear and Dislocation	5.2	3.5	1.4×10^7

Results reported are the mean for each group. For instance, the value in row *Tear*, column *Elongation* shows the average of the ratios of the second eigenvalue to the third eigenvalue for all BGs whose long biceps tendon was diagnosed as torn; the closer the depth and width of the BG are to being the same, the closer to 1 is this measure.

1. Group normal and pathological cases. Each set of thickness fields is assigned a group label according to an expert diagnosis of LBT condition based on evaluation of a magnetic resonance imaging (MRI) of the patient's shoulder. We had six groups: normal, tear, subluxation, dislocation, tear and subluxation, and tear and dislocation.
2. Compute 3D shape measures. Here, we compute three shape measures of interest for each BG. The first is elongation, computed as follows. We first perform principal components analysis (PCA)[17] on the BG surface points yielding three eigenvectors and corresponding eigenvalues. The eigenvalues λ_1, λ_2, and λ_3 represent the variance of the BG surface points in the directions of the eigenvectors (which describe the main directions of variation) for each BG. They give an approximation to each BG by an ellipsoid, where λ_1, λ_2, and λ_3 represent the lengths of the major axes of such an ellipsoid. Computing the three values of the ratios λ_1/λ_2, λ_1/λ_3, and λ_2/λ_3 yields measures of elongation of the object. For a spherical object we expect that $\lambda_1\approx\lambda_2\approx\lambda_3$. For a cylindrical object, we expect that $\lambda_1\gg\lambda_2\approx\lambda_3$, and for a disk-like object we expect that $\lambda_1\approx\lambda_2\gg\lambda_3$. Figure 13 illustrates the elongation measurement with two example BGs. The second shape measure we compute is surface irregularity, which is computed as follows. We compute the centroid of all of the BG surface points, and compute the mean Euclidean distance from each surface point to this centroid, as a measure of size. We then compute the standard deviation of these distances as a measure of surface roughness. The third shape measure is a 3D moment invariant, which has been shown to be invariant to translation and rotation.[18] It is defined as follows:

$$J_1 = \mu_{200} + \mu_{020} + \mu_{002}$$

$$\mu_{pqr} = \sum_x \sum_y \sum_z (x-\overline{x})^p (y-\overline{y})^q (z-\overline{z})^r p(x,y,z),$$

where μ_{pqr} is the 3D central moment;

$$(\overline{x},\overline{y},\overline{z}) = (m_{100}/m_{000}, m_{010}/m_{000}, m_{001}/m_{000})$$

is the centroid of the surface,

$m_{pqr} = \sum_x \sum_y \sum_z x^p y^q z^r p(x,y,z)$ is the 3D moment, and

$$p(x,y,z) = \begin{cases} 1 \text{if} (x,y,z) \text{ is a surface point.} \\ 0 \text{ otherwise.} \end{cases}$$

RESULTS

Validation

Table 1 shows the results of our classification experiment described in "Validation of 3D Shape Representation." Accuracy was over 80% for most classification tasks, although different types of classifiers performed best for different tasks. We experimented with all classifiers in the *PRTools v.4* package,[19] and we obtained best results with a minimum least square linear classifier and a quadratic Bayes normal classifier. The former bases its decision on a linear function

Table 3. Pathology Group Separability

	Elongation	Surface Roughness	3D Moment
Normal/mean (abnormal)	0.7	1.3	2.5
p value	0.02	0.06	0.27

For each measurement, all of the abnormal groups are aggregated by taking the mean. Normals are then compared with abnormals by taking the ratio given in the first row of the table. The second row shows p values resulting from a one-way ANOVA test for each measurement, to test the null hypothesis that there are no significant differences between the means of the normal and pathological groups.

Table 4. The Mean Value of Each Measurement Within Five Different Age Groups

	Elongation	Surface Roughness	3D Moment
30 and under	6.9	4.6	3.8×10^7
31–40	9.5	3.4	1.3×10^7
41–50	6.9	3.5	9.7×10^6
51–60	9.5	3.5	1.4×10^7
61 and over	4.8	3.7	1.5×10^7

We observe a difference in the surface roughness and 3D moment measurements for the 31 and over groups compared with the 30 and under groups.

of the inputs, whereas the latter finds a quadric hypersurface that best separates the classes. For further details, we refer the reader to Fukunaga's book on pattern recognition.[20]

Shape Differences

Table 2 gives the mean, for each group, of the measurements described in "Computing Differences Between Groups." The first row of Table 3 gives the ratio of the measurements for the normal groups against the mean of the measurements for all of the abnormal groups. The purpose of the first row of Table 3 is to yield a picture of the ways in which the groups are different. To test the null hypothesis that there are no statistically significant differences between the groups, we performed a one-way ANOVA test for every measurement type on every thickness field type. Resulting p values are given in the second row of Table 3. We also stratified the measurements according to age in Table 4.

DISCUSSION

Validation

No classifier performed adequately in the diagnosis of medial wall angle abnormalities; we attribute this to the imprecise definition given in previous studies.[3,4,6] Usually, this is given as a diagram (such as Fig. 2), which does not cover frequent cases where the medial wall may have one or more plateaus rather than having a uniform slope (Fig. 14). Also, previous authors are vague regarding the locations of BG measurements; such inconsistencies between studies may have an adverse effect on classification. Considering these obstacles, the results are encouraging in that they suggest that the majority of important BG shape features are captured by our representation. Especially encouraging is the classification performance for the supratubercular ridge of Meyer, which proved to be difficult for the human expert to identify.

Shape Differences

The results in the first row of Table 3 indicate that differences between normals and abnormals, as evidenced by the 3D shape measures taken, range between 30% (for elongation and surface roughness) and 250% (for 3D moment invariant). Some of the p values in the second row of Table 3 are also encouraging. For the measurement of elongation, we can reject the null hypothesis that the means of the groups are the same with 98% confidence. This agrees with what is known about the relationship of BG dimensions to LBT pathology: a deep, narrow groove and a shallow, wide groove; both have a tendency to cause LBT pathology, and both of these conditions are reflected in the elongation measure as it was taken in this work. The confidence of null hypothesis for the surface roughness measure is slightly weaker at 94%, but still encouraging. The 3D moment invariant measure clearly requires further investigation into its usefulness as we can reject the null hypothesis with only 73% confidence with this measure. However, the difference

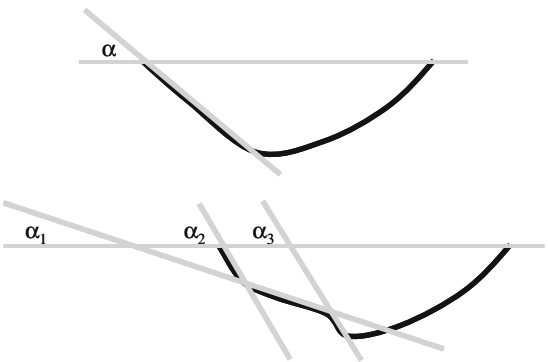

Fig 14. (a) An axial cross section BG whose medial wall has a clearly defined angle α according to the description of this measurement in previous literature (eg, Fig. 2). (b) An example where the medial wall has a "plateau," yielding many conceivable medial wall angle measurements. Previous literature is not precise in describing how these cases are measured.

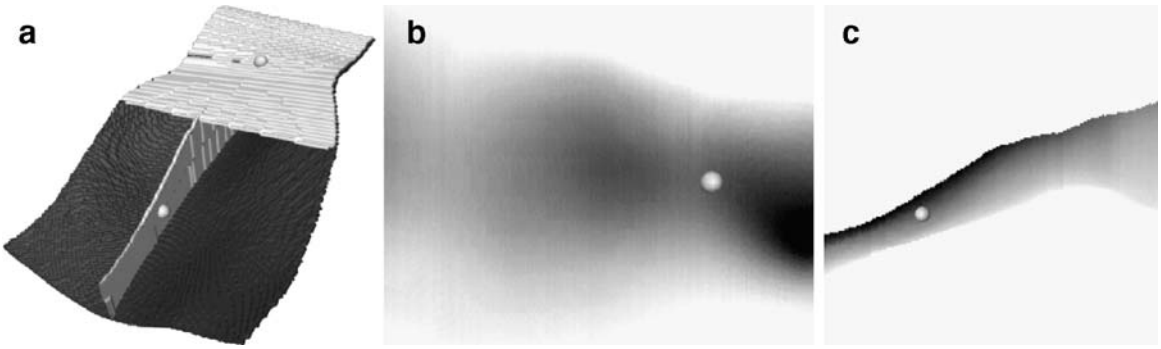

Fig 15. (a) BG visualized with cutaway view of intertubercular sheet and medial sheet. Small spheres indicate 3D positions on the intertubercular sheet and the medial sheet. (b) The small sphere indicates the corresponding 2D location on the visualized depth field. (c) The small sphere indicates the corresponding 2D location on the visualized width field (similar for the medial wall and depth fields).

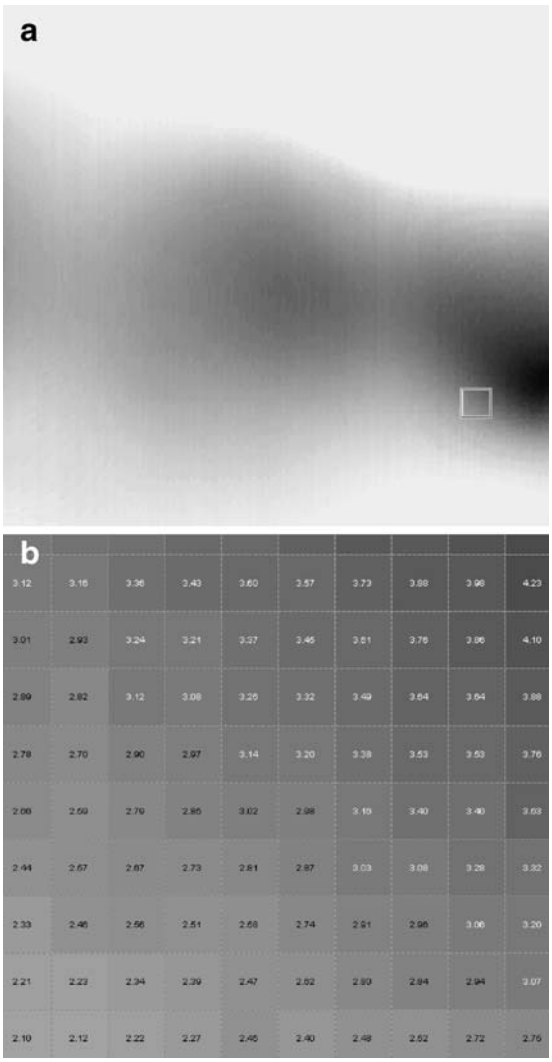

Fig 16. Quantitative exploration of a depth field using MATLAB's *imtool*.[15] (a) The clinician drags a resizable square over the area of interest in the field. (b) Thickness (depth) values, in millimeters, are shown for the area within the square.

between the normals and the mean of the abnormals for the 3D moment invariant measure given in the first row of Table 3 is encouraging enough that we should continue to investigate the properties and value of this measurement of the 3D shape of the BG. In Table 4, the surface roughness and 3D moment measurement show a discernible difference between the 30 and under and the 31 and over groups.

Visualization

Deserving of a brief discussion are the visualization capabilities afforded to the clinician by this 3D shape representation. It is of value to establish visual correspondence between points on the visualized 3D BG surface and points on the thickness fields, as shown in Figure 15, to give the clinician an intuitive sense of how to visualize and navigate the thickness and depth fields. The clinician can then observe, at a glance, qualitative features of depth, width, and medial wall in isolation from one another; something that is difficult to do when simply visualizing the entire BG surface at once. The clinician can, for example, distinguish a rapid widening on the medial wall side of the BG from an overall widening of the BG in a straightforward fashion by observing a rapid change in brightness on the thickness fields. This distinction would be of clinical interest because it is known that the slope of the medial wall has a strong impact on the tendency for LBT subluxation and dislocation.[1] Should the clinician wish to explore the fields qualitatively, this shape representation permits such exploration using tools such as Matlab's *imtool*,[21] as shown in Figure 16. The clinician can browse to an area of interest in the field, zoom it in tightly, and see corresponding thickness values in physical units.

CONCLUSION

In this paper, we have presented a novel 3D shape representation for the bicipital groove of the proximal humerus. We have detailed the computation of the representation from a 3D BG surface and have validated the accuracy of the shape descriptor in capturing characteristics of BG shape that have been reported in previous 2D studies. We then computed several 3D characteristics of shape based on the shape descriptor and showed that these measures distinguish well between patients with normal, healthy long biceps tendons and those whose tendons are torn, subluxated, dislocated, or some combination of these abnormalities. We also showed that the shape descriptor permits both qualitative and quantitative exploration of the BG in ways not possible in 2D, allowing the clinician to explore aspects of BG depth, width, and medial wall in isolation from one another. Future work in this area could include use of these shape characterizations to perform handedness identification in individuals for forensic science; it is understood that handedness may play a role in determining the shape of the BG.[22]

REFERENCES

1. Bateman JE: The Shoulder and Neck. USA: W. B. Saunders Company, 1978

2. Meyer AW: Spontaneous dislocation and destruction of tendon of long head of biceps brachii. Fifty-nine instances. Arch Surg 17:493–506, 1928

3. Hitchcock HH, Bechtol CO: Painful shoulder. Observations on the role of the tendon of the biceps brachii in its causation. J Bone Jt Surg Am 30A:263–273, 1948

4. Ueberham K, Le Floch-Prigent P: Intertubercular sulcus of the humerus: biometry and morphology of 100 dry bones. Surg Radiol Anat 20(5):351–354, 1998

5. Pfahler M, Brenner S, Refior H: The role of the bicipital groove in tendopathy of the long biceps tendon. J Bone Jt Surg 8(5):419–424, 1999

6. Ahovuo J: Radiographic anatomy of the intertubercular groove of the humerus. Eur J Radiol 5(2):83–86, 1985

7. Robertson DD, Yuan J, Bigliani LU, Flatow EL, Yamaguchi K: Three-dimensional analysis of the proximal part of the humerus: relevance to arthroplasty. J Bone Jt Surg Am 82-A(11):1594–1602, 2000

8. Itamura J, Dietrick T, Roidis N, Shean C, Chen F, Tibone J: Analysis of the bicipital groove as a landmark for humeral head replacement. J Bone Jt Surg 11(4):322–326, 2002

9. Blum H: A transformation for extracting new descriptors of shape. In: Whaten-Dunn W Ed. Models for the Perception of Speech and Visual Form. Cambridge, USA: MIT Press, 1967, pp 362–380

10. Pizer S, Fletcher PT, Joshi S, Thall A, Chen JZ, Fridman Y, Fritsch DS, Gash AG, Glotzer JM, Jiroutek MR, Lu C, Muller KE, Tractor G, Yushkevich P, Chaney EL: Deformable M-reps for 3D medical image segmentation. IJCV 55(2–3):85–106, 2003

11. Heijden F, Duin RPW, Ridder D, Tax DMJ: Classification, Parameter Estimation and State Estimation: An Engineering Approach Using Matlab. USA: John Wiley and Sons, 2004

12. van Leersum M, Schweitzer ME: Magnetic resonance imaging of the biceps complex. Magn Reson Imaging Clin N Am 1(1):77–86, 1993

13. Cervilla V, Schweitzer ME, Ho C, Motta A, Kerr R, Resnick D: Medial dislocation of the biceps brachii tendon: appearance at MR imaging. Radiology 180(2):523–526, 1991

14. Jain AK: Fundamentals of Digital Image Processing. USA: Prentice Hall, New Jersey, 1989

15. Duda RO, Hart PE: Use of the Hough transformation to detect lines and curves in pictures. Commun ACM 15:11–15, 1972

16. Goodall C: Procrustes methods in the statistical analysis of shape. J R Stat Soc B 53(2):285–339, 1991

17. Jolliffe IT: Principal Components Analysis. New York, USA: Springer-Verlag, 1986

18. Sadjadi FA, Hall EL: Three-dimensional moment invariants. IEEE PAMI 2(2):127–136, 1980

19. Delft University of Technology: PRTools 4. http://www.prtools.org, 2005

20. Fukunaga K: Introduction to Statistical Pattern Recognition, 2nd edition. Boston: Academic Press, 1990

21. The MathWorks, Inc.: Matlab 7.0.4.365 R14 SP2, 1984–2005

22. Selveraj KG, Selvakuhmarb V, Indrasingh I, Chandib G: Handedness identification from intertubercular sulcus of the humerus by discriminant function analysis. Forensic Sci Int 98:101–108, 1998